Bituminous Mixtures Simulation With Distinct Particle Elements Method

Dondi G.
Professor – University of Bologna – DISTART Strade

Bragaglia M.
PhD Student – University of Bologna – DISTART Strade

Vignali V.
PhD Student – University of Bologna – DISTART Strade

Synopsis

This paper investigates the use of Distinct Particle Elements Method (*DEM*) to simulate the behaviour of a bituminous mixture in a Marshall test.
To investigate the effect of particles number on material properties two different specimen generation procedures have been implemented: the up-scaling technique, that allows to enlarge the particles diameter with a great reduction of their number and consequently of the computational times, and the cluster logic, that allows to schematize aggregates with group of particles of arbitrary shape that are physically bonded together.
For each test the stability-flow curve and the stresses in the specimen have been investigated.
To point out *DEM* particular features in performance related modelling of asphalt concrete tests, the laboratory results have been reproduced also with a finite difference code.

Bituminous Mixtures Simulation With Distinct Particle Elements Method

INTRODUCTION

The Distinct Particle Element Method (*DEM*) for modelling the movement and interaction of assemblies of rigid spherical particles subjected to external stresses was developed by Cundall and Strack (1979). Although the *DEM* has been applied to model the behaviour of soils and granular materials (Cundall & Strack, 1979; McDowell & Harireche, 2002), it has not been widely used to investigate the mechanical behaviour of bituminous mixtures.

The traditional approach to modelling asphaltic materials is to treat them at the macro-scale using continuum models based on the Finite Element Method (Collop et al., 2004). It requires the division of the problem domain into a collection of elements of standard shapes (triangle, quadrilateral, tetrahedral, etc.). The continuum assumption implies that at all points in the problem domain the materials cannot broken into pieces; all points originally in the neighbourhood of a certain area remain in the same neighbourhood throughout the deformation process (Jing, 2003).

A *DEM* model instead is composed of distinct particles that displace independently from one another and interact only at contact points. Their interaction is treated as a dynamic process with states of equilibrium developing whenever the internal forces balance. The contact forces and displacements of a stressed assembly of particles are found by tracing the movements of the individual ones.

The calculations performed in *DEM* alternate between the application of Newton's second law to the particles and a force-displacement law at the contacts (figure 1). The first is used to determine the motion of each particle arising from the contact and body forces acting upon it, while the second is used to update the contact forces arising from the relative motion at each contact.

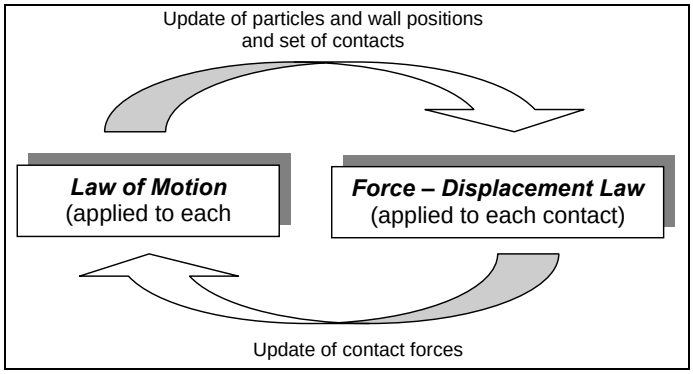

Figure 1: Calculation cycle in *DEM*

A contact model, that describes the physical behaviour occurring at a contact, is composed of three parts:

- a contact-stiffness model, that provides a relation between the normal (F_n) and shear (F_s) components of contact forces and the relative displacements (U_n, U_s). The most diffused for his simplicity is the linear model, in which the forces and displacements are linearly related by the contact stiffness (k_n, k_s):

$$F_n = k_n \cdot U_n \quad (1)$$

$$F_s = -k_s \cdot U_s \quad (2)$$

- a slip and separation model: the slip condition occurs when the shear component of force (F_s^i) reaches and exceeds the maximum allowable shear contact force ($F_s^{\max}$). This value is taken to be the minimum friction coefficient of the two entities in contact (μ) multiplied by the magnitude of the compressive normal component of force (F_n^i):

$$F_s^i \geq F_s^{\max} = \mu \cdot \left| F_n^i \right| \quad (3)$$

- a bonding model: the contact bond reproduce the effect of an adhesion acting over the vanishingly small area of the contact point (figure 2).

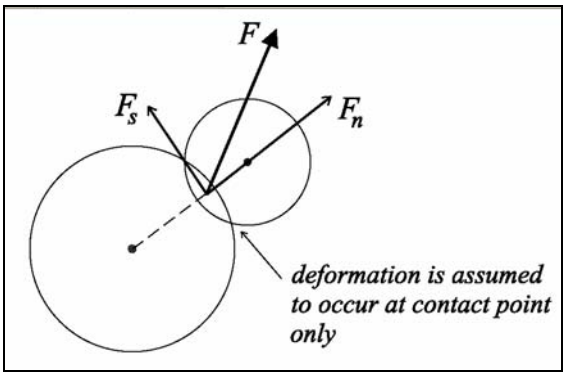

Figure 2: Contact scheme

The Distinct Particles Element Method is very suitable to model the interaction of discrete objects subjected to large displacements or failure processes, because, differently from the continuum methods, it is possible to investigate the system evolution after the failure, over which the domain separation in blocks is admitted.
Since the objective of this paper is to simulate a Marshall test using the *DEM* approach, it has been necessary to generate first a specimen that replicates the laboratory asphalt mixture and second a suitable test equipment.

NUMERICAL SAMPLE PREPARATION PROCEDURE

Particles Generation

The models parameters have been determined by comparing experimental Marshall results with the numerical ones. In according with the granulometric curve of the lab mixture (figure 3), after modelling of the breaking heads by a ring of 100 mm diameter, three different particles generation procedures have been performed:

- the first, based on circular particles. In this way six specimens have been modelled, generating first the particles held to 10 UNI sieve and then the others;
- the second, based on cluster logic, that, allowing to schematize particles with group of elements of not circular but arbitrary shape, are more representative of asphalt concrete aggregates;
- the third, based on up-scaling technique (Hainbüchner et al, 2003).

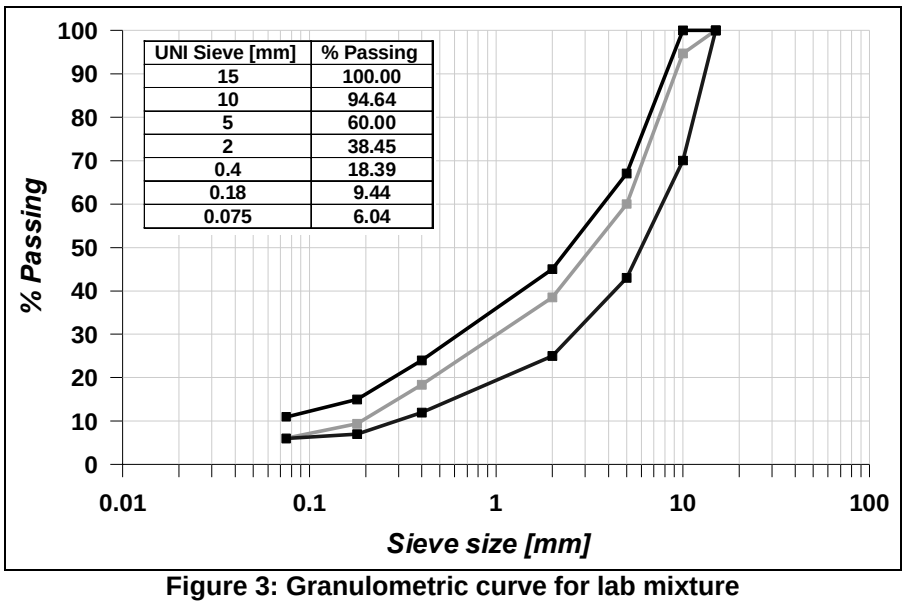

Figure 3: Granulometric curve for lab mixture

In figure 4 the model with 58000 particles (called *H 58000*) is represented.

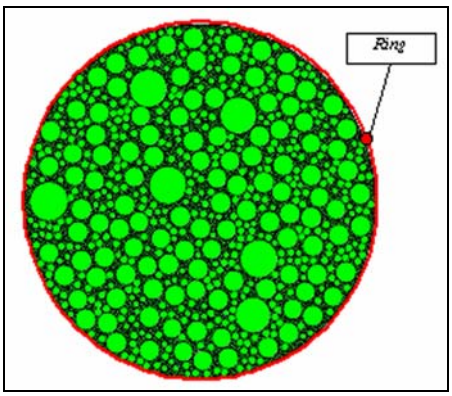

Figure 4: H 58000 model

The up-scaling technique consist of multiplying the particles diameter for a factor *S*. In this case: $S = 10$. So the up-scaled granulometric curve has the same shape of laboratory one, but it is shifted of a value (*ΔD*) given by the following formula:

$$\Delta D = \left(S - 1 \right) \cdot D_{ini} \tag{4}$$

where *S* is the up-scaling factor and D_{ini} is the medium dimension of the laboratory granulometric curve.

The measured and modelled properties values are shown in table 1, where each mixture is called by her particles number.

Table 1: Granulometric parameters of the modelled mixtures

Model	**A 100**	**B 200**	**C 600**	**D 2000**	**E 11500 (Cluster)**	**G 21000**	**H 58000**	**Up-scaled Model**	**F 20000**
Particles number	113	215	655	2285	11472	21626	58429	**Particle number**	20385
D_{sieve} [mm]	Passing [%]	Passing [%]	Passing [%]	Passing [%]	Passing [%]	Passing [%]	Passing [%]	**D_{sieve} [mm]**	Passing [%]
15	100	100	100	100	100	100	100	**150**	100
10	39	43	47	48	70	93	93	**100**	95
5	3	10	15	18	45	48	50	**50**	60
2			6	9	25	25	27	**20**	39
0.4				3		10	12	**4**	18
0.18						4	7	**1.8**	9
0.075								**0.75**	6

In figure 5 some of laboratory and modelled granulometric curves are represented.

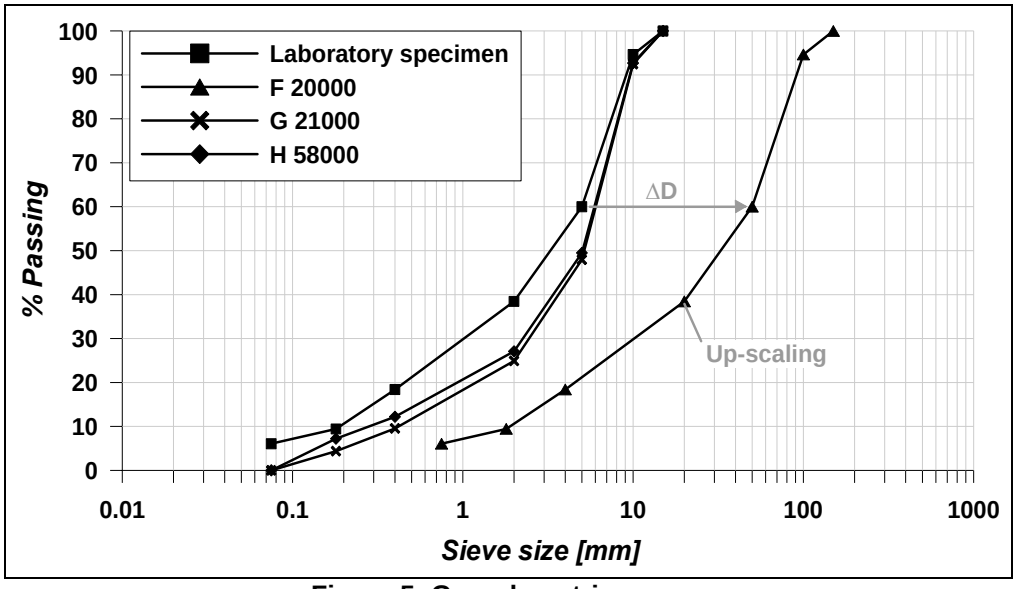

Figure 5: Granulometric curves

Contact Models Definition

The bitumen of the laboratory mixture is a 50/70 PG.

Each mix, except the *E 11500* generated with cluster logic, was numerically modelled with the Burger's model shown in figure 6. It comprises a spring and dashpot in parallel, connected in series to a spring and dashpot in series. It can readily be shown that the time dependent stiffness of the Burger's model in *i* direction is given by (Collop et al., 2004):

$$k_i = \left[\frac{1}{K_0^i} + \frac{t}{C_\infty^i} + \frac{1}{K_1^i}\left(1 - e^{-t/\tau^s}\right) \right]^{-1} \quad (5)$$

where:

t is the loading time;

$K_0^{\ i}$ is the modulus of the spring connected in series;

$K_1^{\ i}$ is the modulus of the spring connected in parallel;

$C_\infty^{\ i}$ is the viscous damping constant of the dashpot connected in series;

$C_1^{\ i}$ is the viscous damping constant of the dashpot connected in parallel;

$\tau^s = C_1^s / K_1^s$ is the relaxation time.

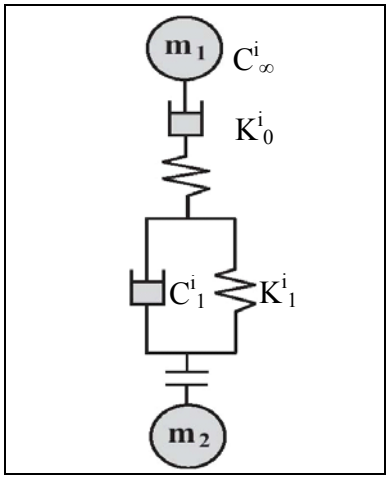

Figure 6: *Burger*'s model

The normal (k_n) and shear (k_s) contact stiffnesses have been estimated from shear modulus (*G'*), bulk modulus (*K'*) and Poisson ratio (*v*) of the laboratory specimen (table 2), as follows (Cundall & Al., 2003):

$$k_n = K' \frac{4\pi \Sigma R^2}{(1-n)\Sigma R \Sigma L} \quad (6)$$

$$k_s = G' \frac{8\pi \Sigma R^2}{(1-n)\Sigma R \Sigma L} - k_n \quad (7)$$

where:

n is the porosity;

L is the distance between the centre of gravity of two particles in contact;

R is the particle medium radius.

Table 2: Properties of the laboratory mixture (temperature = 60°C)

ρ [Kg/m^3]	***v***	***K'*** [MPa]	***E'*** [MPa]	***G'*** [MPa]
2322	0.15	450	945	411

The model parameters have been chosen arbitrarily to obtain predicted stability-flow curves similar in magnitude and shape to measured data. Table 3 contains the contact stiffnesses values and the Burger's model properties of the numerical tests; figure 7 shows the regression curves of normal (k_n) and shear (k_s) contact stiffnesses versus particles number.

Table 3: Contact stiffnesses values and *Burger* model parameters of the numerical tests (T = 60°C)

Model	*Normal stiffness*					*Shear stiffness*				
	MN/m	MN/m	MN/m	MNs/m	MNs/m	MN/m	MN/m	MN/m	MNs/m	MNs/m
	C^n_1	K^n_0	K^n_1	C^n_∞	k_n	C^s_1	K^s_0	K^s_1	C^s_∞	k_s
A 100	$7.9\cdot10^{2}$	$1.6\cdot10^{1}$	$1.6\cdot10^{1}$	$3.2\cdot10^{2}$	$\mathbf{1.5\cdot10^{1}}$	$7.9\cdot10^{2}$	$2.0\cdot10^{3}$	$4.0\cdot10^{3}$	$3.2\cdot10^{2}$	$\mathbf{2.1\cdot10^{1}}$
B 200	$2.5\cdot10^{2}$	$1.6\cdot10^{1}$	$1.6\cdot10^{1}$	$1.0\cdot10^{2}$	$\mathbf{7.7\cdot10^{0}}$	$7.9\cdot10^{2}$	$2.5\cdot10^{4}$	$5.0\cdot10^{4}$	$3.2\cdot10^{2}$	$\mathbf{6.0\cdot10^{0}}$
C 600	$2.5\cdot10^{2}$	$1.6\cdot10^{1}$	$1.6\cdot10^{1}$	$1.0\cdot10^{2}$	$\mathbf{2.8\cdot10^{0}}$	$3.1\cdot10^{2}$	$2.5\cdot10^{4}$	$5.0\cdot10^{4}$	$1.3\cdot10^{2}$	$\mathbf{2.3\cdot10^{0}}$
D 2000	$2.5\cdot10^{1}$	$1.6\cdot10^{1}$	$1.6\cdot10^{1}$	$1.0\cdot10^{1}$	$\mathbf{1.4\cdot10^{0}}$	$7.9\cdot10^{3}$	$2.5\cdot10^{2}$	$5.0\cdot10^{2}$	$3.2\cdot10^{3}$	$\mathbf{1.1\cdot10^{0}}$
E 11500	$7.9\cdot10^{0}$	$7.9\cdot10^{0}$	$7.9\cdot10^{0}$	$1.0\cdot10^{1}$	$\mathbf{2.8\cdot10^{-1}}$	$2.5\cdot10^{3}$	$5.0\cdot10^{4}$	$1.0\cdot10^{5}$	$1.0\cdot10^{2}$	$\mathbf{2.2\cdot10^{-1}}$
G 21000	$1.9\cdot10^{3}$	$2.5\cdot10^{2}$	$2.5\cdot10^{2}$	$3.2\cdot10^{2}$	$\mathbf{1.2\cdot10^{-1}}$	$1.9\cdot10^{1}$	$2.5\cdot10^{6}$	$2.5\cdot10^{6}$	$3.2\cdot10^{0}$	$\mathbf{1.1\cdot10^{-1}}$
H 58000	$1.9\cdot10^{3}$	$2.5\cdot10^{2}$	$2.5\cdot10^{2}$	$3.2\cdot10^{2}$	$\mathbf{5.6\cdot10^{-2}}$	$1.9\cdot10^{1}$	$2.5\cdot10^{7}$	$2.5\cdot10^{7}$	$3.2\cdot10^{0}$	$\mathbf{4.6\cdot10^{-2}}$
F 20000	$1.9\cdot10^{3}$	$2.5\cdot10^{2}$	$2.5\cdot10^{2}$	$3.2\cdot10^{2}$	$\mathbf{1.8\cdot10^{-1}}$	$1.9\cdot10^{1}$	$2.5\cdot10^{6}$	$2.5\cdot10^{6}$	$3.2\cdot10^{0}$	$\mathbf{1.6\cdot10^{-1}}$

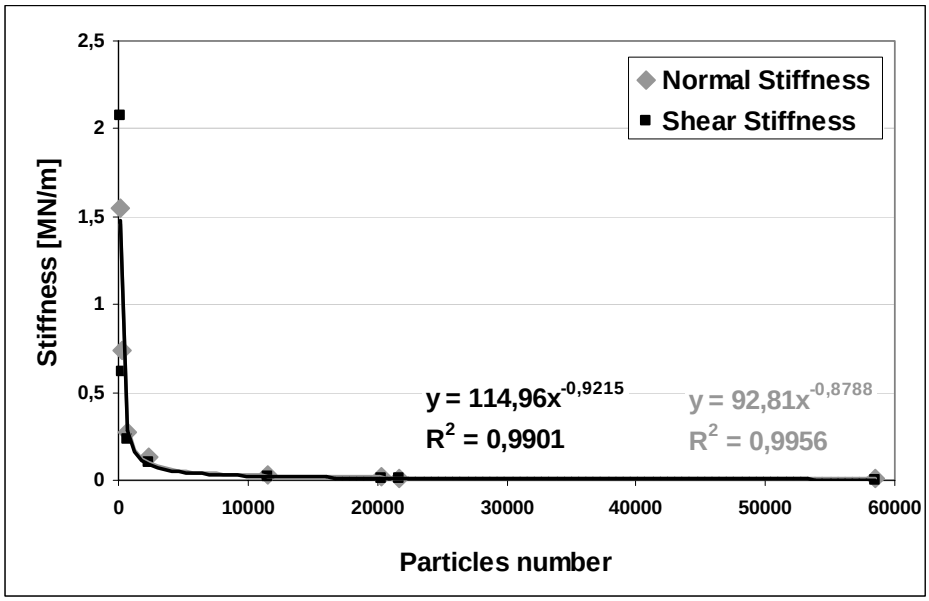

Figure 7: Regression curves of normal and shear stiffness versus particles number

The contact friction coefficient (μ) has been estimated from the friction angle of the aggregates of the laboratory mixture ($\phi = 35°$). In this case: $\mu = 0.8$.

LABORATORY EQUIPMENT MODELLING

After the sample generation, the numerical test have been carried out by moving the upper and lower breaking heads in the vertical direction with a constant velocity of 0.425 mm/sec (figure 8). The coefficient of friction between the loading plates and the sample was set to be zero.

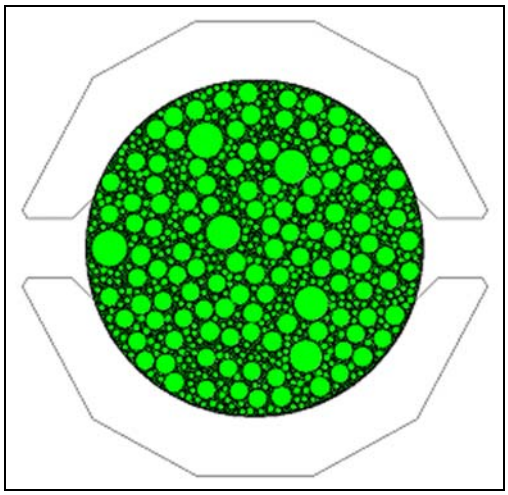

Figure 8: General model set-up of Marshall test

For each test the stresses on the horizontal and vertical medium planes in the specimen have been investigated through measurement circles of 5.08 mm radius (figure 9).

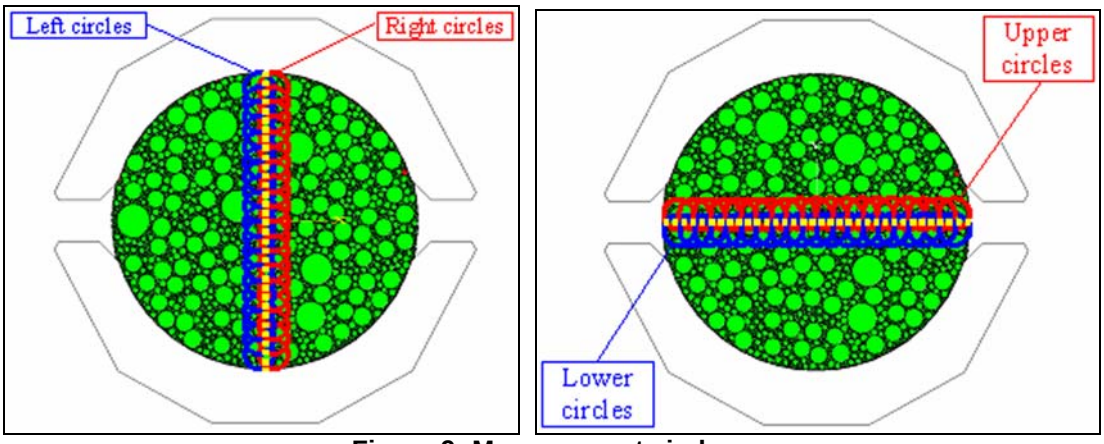

Figure 9: Measurement circles

MODELLING RESULTS

For each test the following quantities have been monitored:

- stability-flow curves;
- contact forces distribution inside the specimen;
- shear and normal stresses inside measurement circles represented in figure 9.

Table 4 and figure 10 show stability-flow curves obtained by models.

Table 4: Stability and flow values of modelled specimens

	Laboratory specimen	*A 100*	*B 200*	*C 600*	*D 2000*	*E 11500*	*G 21000*	*H 58000*	*F 20000*
Stability (S) [N]	12411	12948	13652	13451	13522	13416	12834	12951	12099
Flow (s) [mm]	2.20	1.56	1.94	2.52	2.10	2.58	2.86	2.23	2.35

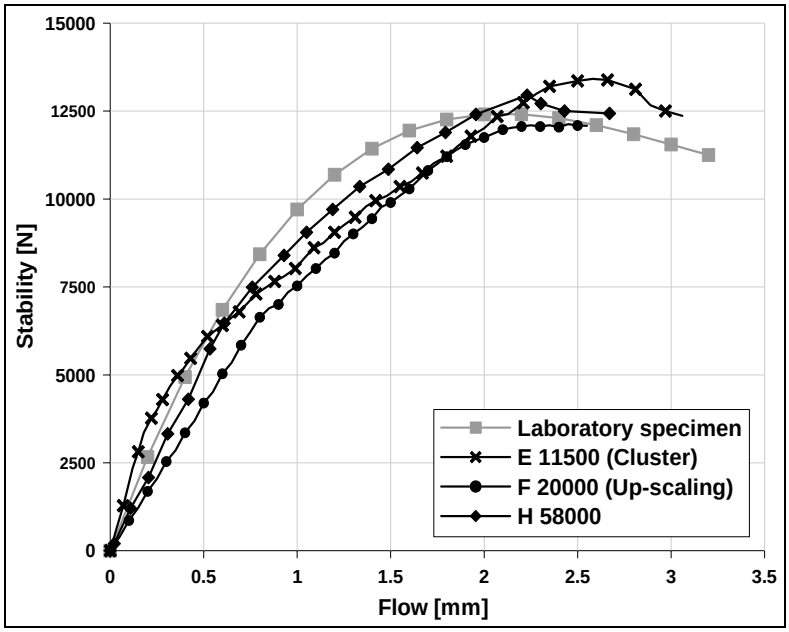

Figure 10: Stability-Flow Curves

There is a good agreement between numerical results and experimental behaviour of asphalt concrete. All tests, independently of stability value, show the same trend: a first elastic segment, in which load and displacement are linear dependent, and a second visco-elastic behaviour. The visco-plastic component is absent because the contact model adopted in this case does not provide for it.

The analysis of the contact forces distribution inside the specimen for flow corresponding to stability show an axial symmetry (figure 11). The contact forces increase to growth of particles number.
During the laboratory tests the load applied to the specimen by breaking heads induces inside asphalt concrete a stress state which spreads inside the sample immediately, with a velocity higher than the modelled tests. In this case, in fact, the stresses produced by loading head share out among particles from sample perimeter to centre. The velocity of the stress wave, which depends of contact stiffnesses, has been estimated from equations (1), (2) and (5) as follows:

$$v_i = \frac{\Delta F_i}{\Delta s_{r,i}} = k_i \cdot \Delta l = \left[\frac{1}{K_0^i} + \frac{v_{r,i}}{s_{r,i} \cdot C_\infty^i} + \frac{1}{K_1^i} \cdot \left(1 - e^{-\frac{v_{r,i}}{s_{r,i} \cdot \tau^i}} \right) \right]^{-1} \cdot s_{r,i} \qquad (8)$$

where $s_{r,i}$ and $v_{r,i}$ are respectively the relative displacement and the relative velocity between two adjacent particles.
By equation (8), supposing that the particles displacement and velocity decrease linearly from breaking heads to specimen centre, it has been evaluated $s_{r,i}$, $v_{r,i}$ and the value of flow (s_d) corresponding to stability that takes into consideration the stress wave delay (table 5). It is measured on the medium horizontal plane.

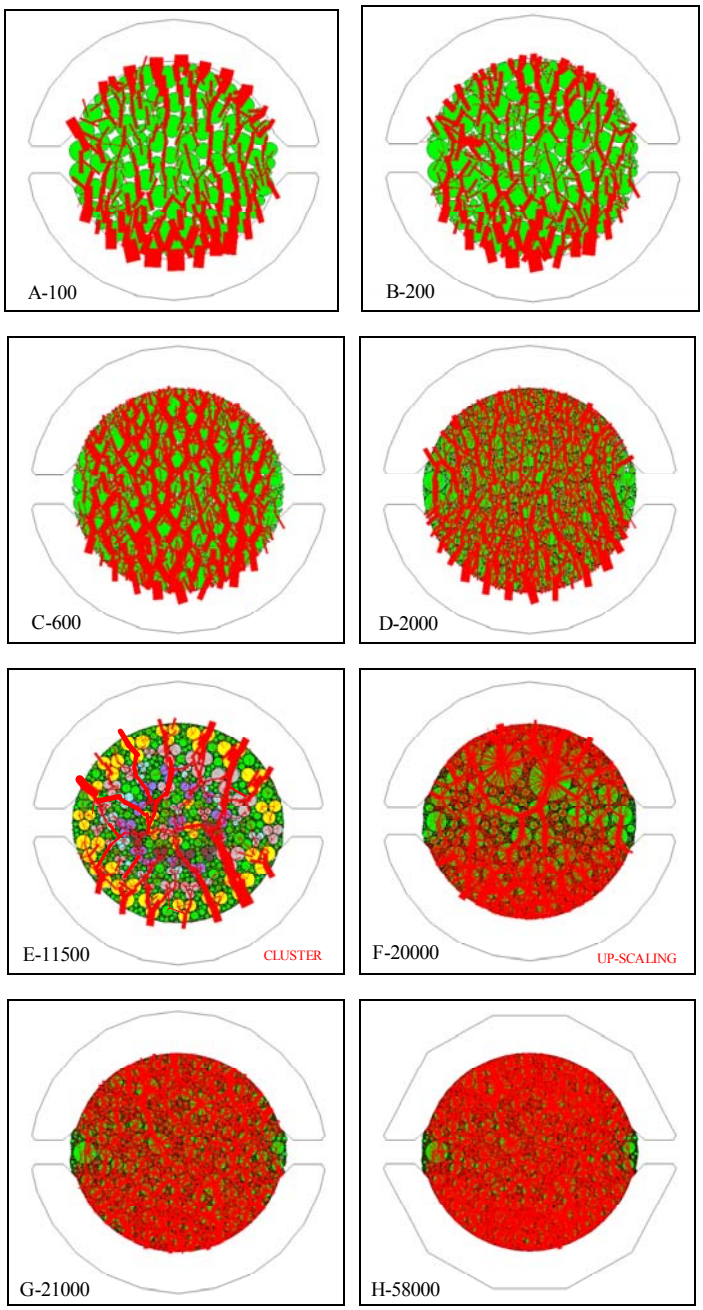

Figure 11: Contact forces distribution inside the specimen for flow corresponding to stability

Table 5: $v_{r,i}$, $s_{r,i}$ and s_d values of modelled specimens

Model	Stability *[N]*	$v_{r,i}$ *[mm/s]*	$s_{r,i}$ *[mm]*	s_d *[mm]*
A 100	12948	$3.2 \cdot 10^{-3}$	1.01	4.70
B 200	13652	$3.2 \cdot 10^{-3}$	0.92	6.20
C 600	13451	$2.9 \cdot 10^{-3}$	0.73	9.59
D 2000	13522	$1.4 \cdot 10^{-3}$	0.47	12.18
E 11500	13416	$1.1 \cdot 10^{-3}$	0.20	11.58
G 21000	12834	$3.7 \cdot 10^{-4}$	0.08	7.00
H 58000	12951	$1.3 \cdot 10^{-4}$	0.03	4.21
F 20000	12099	$5.0 \cdot 10^{-4}$	0.11	9.21

For each test it has been measured the vertical and horizontal stresses distribution inside circles shown in figure 9, for flow corresponding to s_d (figures 12 and 13). The areas subtended by the curves represent respectively the vertical (F_V) and horizontal (F_H) stress resultants. The first one has been compared with stability values (ΔF_V) (table 6).

Table 6: Vertical and horizontal stresses resultant

Model	$D_{Vertical}$	$D_{Horizontal}$	
	F_H *[N]*	F_V *[N]*	ΔF_V *[%]*
A 100	2541	13870	7.12
B 200	3793	14025	2.73
C 600	3525	14811	10.11
D 2000	5221	13227	2.18
E 11500	6193	13957	4.03
G 21000	12507	12988	1.20
H 58000	12356	12561	3.01
F 20000	11825	12110	0.09

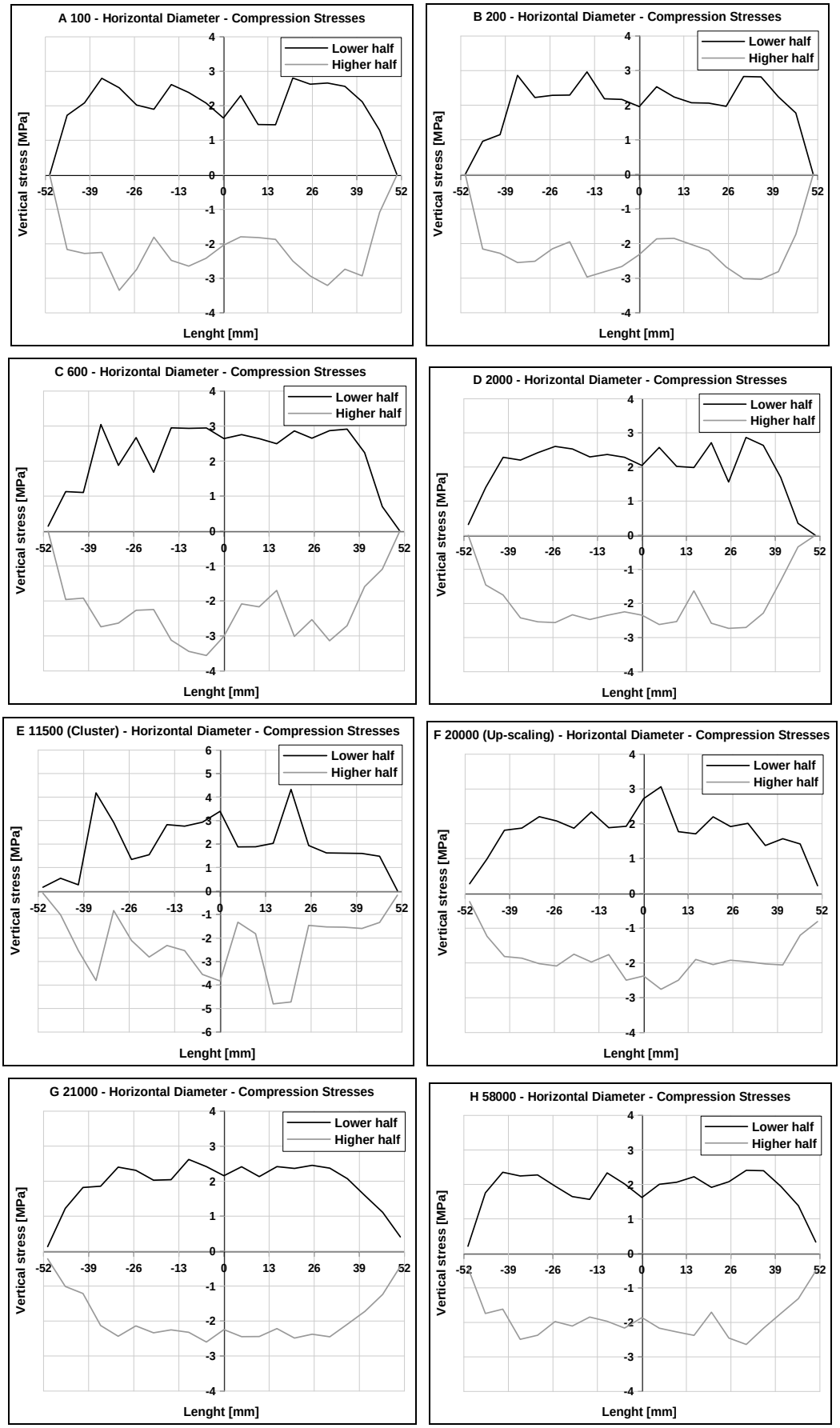

Figure 12: Compression stresses on horizontal diameter for flow corresponding to s_d

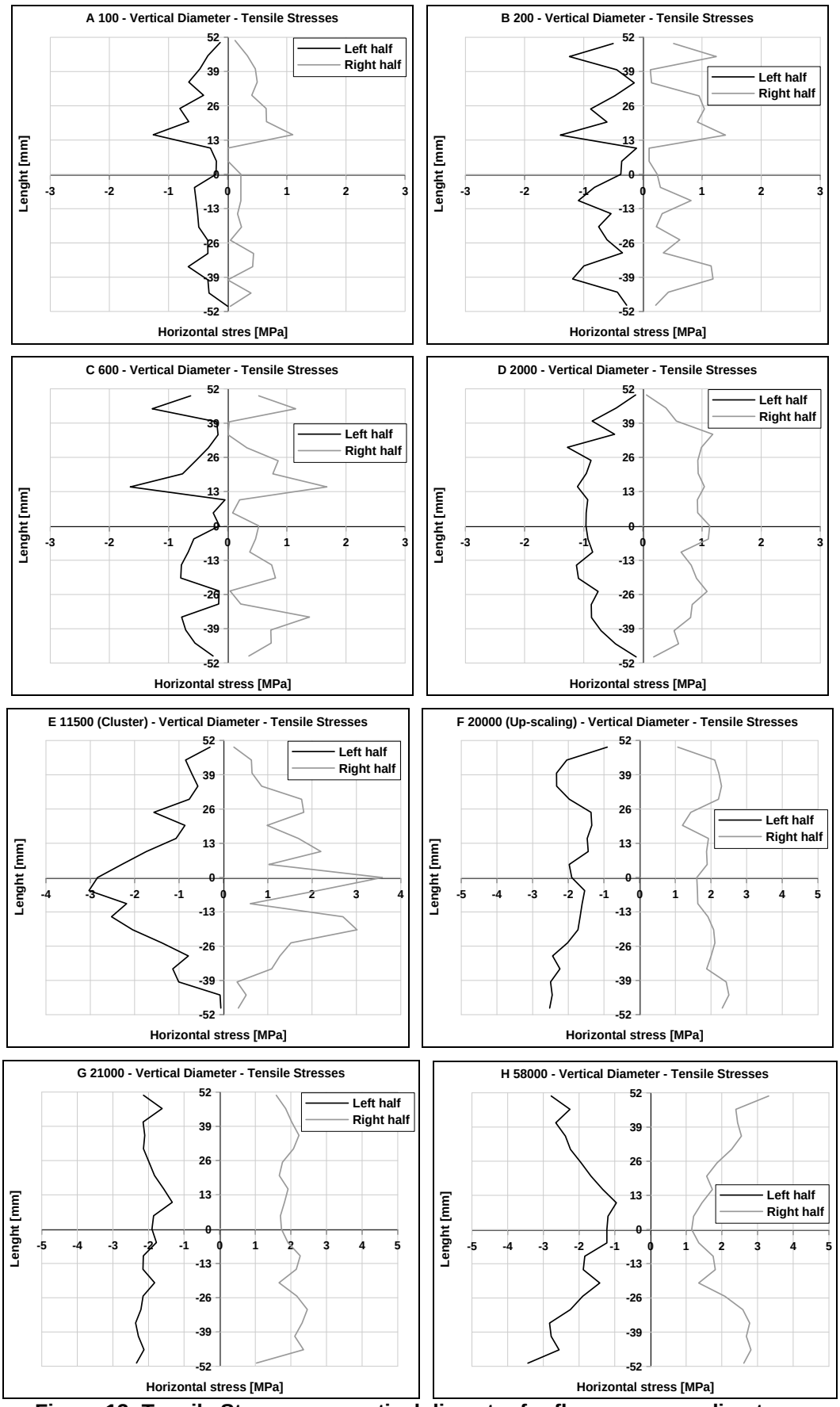

Figure 13: Tensile Stresses on vertical diameter for flow corresponding to s_d

From difference between s_d and s values ($s' = s_d - s$) it is possible to evaluate the stress wave delay. This is a function of particles number, as indicate in figure 14.

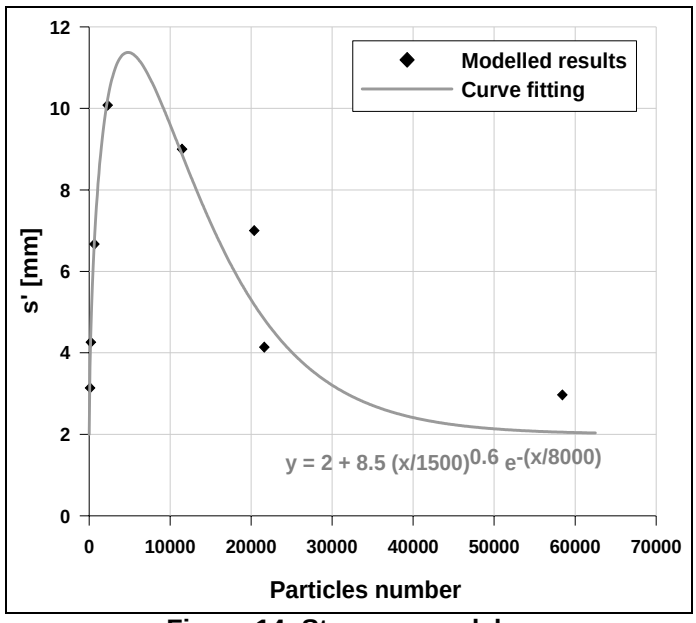

Figure 14: Stress wave delay

To identify the model that shows the better agreement with the experimental results, stability-flow curves reported in figure 10 have been studied. Table 7 and figure 15 show the comparison between laboratory and modelled data in terms of stability (*S*) and flow (*s*).

Table 7: Comparison between experimental and modelled data

	Laboratory specimen	***Modelled specimens***							
		A 100	***B 200***	***C 600***	***D 2000***	***E 11500***	***G 21000***	***H 58000***	***F 20000***
S [N]	12411	12948	13652	13451	13522	13416	12834	12951	12099
ΔS [%]	-	**4.33**	**10.00**	**8.38**	**8.95**	**8.10**	**3.40**	**4.35**	**2.51**
s [mm]	2.20	1.56	1.94	2.52	2.10	2.58	2.86	2.23	2.35
Δs [%]	-	**29.09**	**11.82**	**14.55**	**4.55**	**17.27**	**30.00**	**1.36**	**6.81**

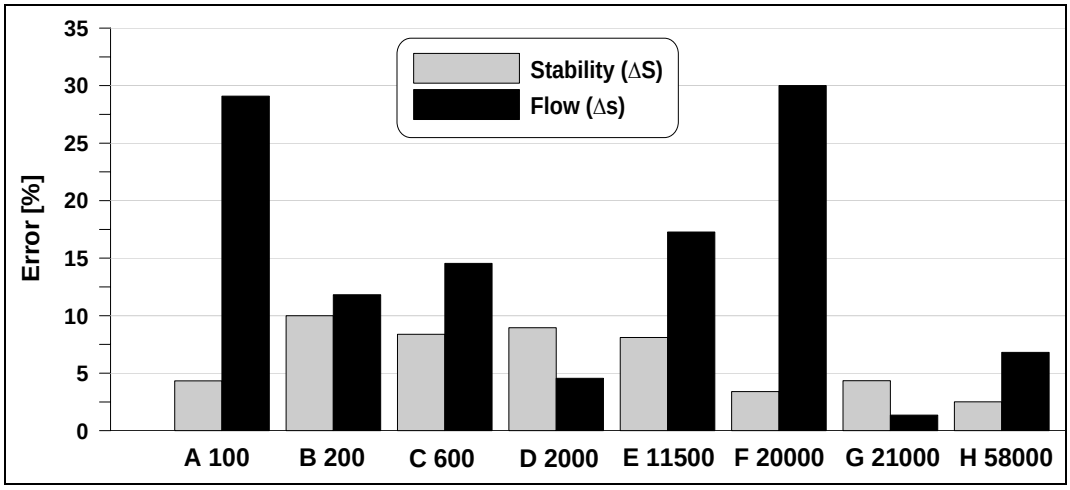

Figure 15: Comparison between measurement and calculated results

Tests results shows that the best model is *H 58000*: in this case predicted and measured curves are similar in magnitude and shape. Stability and flow calculated are respectively 4.35% and 1.36% higher than those calculated for laboratory specimen.

To point out *DEM* particular features for the performance related modelling of asphalt concrete tests, the laboratory results have been reproduced with a finite difference code.

It has been modelled a grid with a circular boundary of 100 mm radius (figure 16). A uniform velocity of 0.85 mm/sec has been applied in the y-direction at the upper semicircle to induce sample compression. At each

zone it has been assigned a Mohr-Coulomb model, with the same constitutive properties of lab sample (table 2). For defining cohesion (C) and angle of friction (ϕ) of the asphalt mixture the "C-ϕ Model" has been used (Fwa et al., 2001). This illustrates a link between Marshall results and the triaxial test properties of C and ϕ as follows:

$$S = -14 + 0.0447C + 0.496\phi \quad (9)$$

$$s = 15.1 + 0.00639C - 6.3444 \log E \quad (10)$$

where:
S is Marshall stability [kN];
s is the Marshall flow [mm];
C is the cohesion [kPa];
ϕ is the angle of friction [°];
E is the elastic modulus [MPa].
In this case C = 935.42 kPa and ϕ = 31.1°.

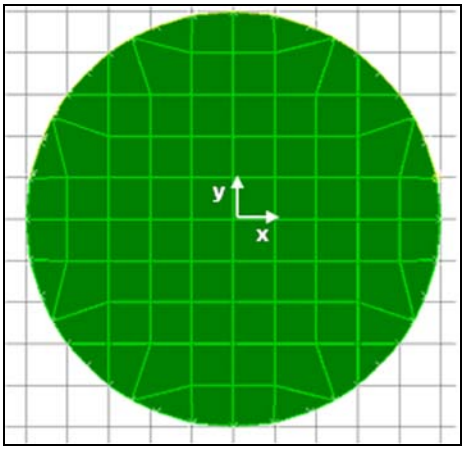

Figure 16: Sample modelled by finite difference code

For the modelled specimen, called *FD*, the stability-flow curve has been compared with laboratory and *H 58000* results (table 8 and figure 17). The two modelled specimens show approximately the same flow, but *FD* stability is smaller than *H 5800* and experimental values.

Table 8: Comparison between experimental, *H 58000* and *FD* data

	Laboratory specimen	***H 58000***	***FD***
S [N]	12411	12951	9151
s [mm]	2.20	2.23	2.00

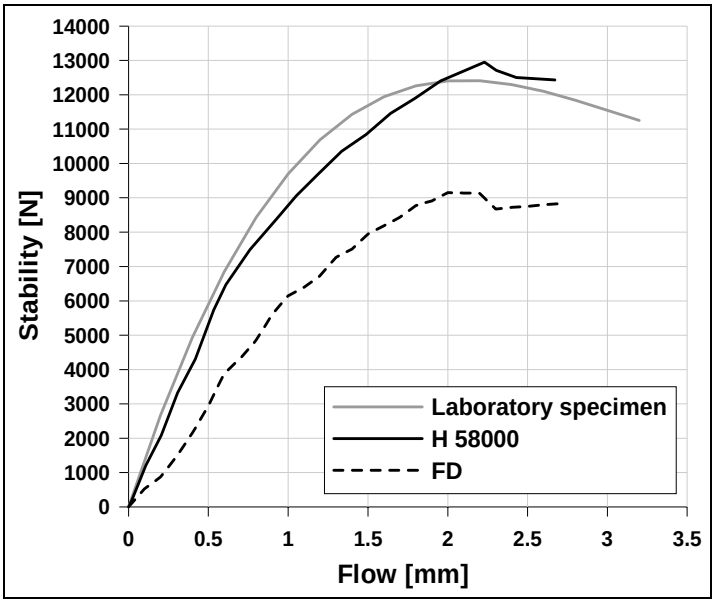

Figure 17: Comparison between stability-flow curves of *FD, H 58000* and lab mix

The comparison between measured and calculated stability-flow curves points out the power of *DEM* approach. Knowing the relationships between the mechanical macroscopic behaviour and the microscopic parameters of the model, *DEM* well supports the researcher in the laboratory tests phase for the mixture optimization as well as for the implementation of new methods for studying the asphalt fatigue resistance in pavements.

CONCLUSIONS

Based upon the developed research work, the following concluding remarks can be stated:

- the *DEM* approach has been used to model the behaviour of asphalt mixtures in a Marshall test;
- to investigate the effect of particles number on material properties the up-scaling technique and the cluster logic have been performed. By the second, in particular, more complex particle shapes can be generated and a graded aggregate can be simulated more realistically without sacrificing computational time;
- a Burger's model was introduced to give a time dependent shear and normal contact stiffnesses;
- the comparison between lab and numerical results show remarkable agreement. The modelled experiments are able to reproduce the main features of a Marshall test, both in qualitative and quantitative manner. The mayor difficulty is relate observed behaviour to the micromechanics of the materials.
- knowing the relationships between the mechanical macroscopic behaviour and the microscopic parameters of the model, *DEM* well supports the researcher in the laboratory tests phase for the mixture optimization.

REFERENCES

1. C.N.R. (1973), "Determinazione della stabilità e dello scorrimento di miscele di bitume e inerti lapidei a mezzo dell'apparecchio Marshall", B.U. n. 30;
2. Collop A.C., McDowell G.R. & Lee Y. (2004), "Use of the distinct element method to model the deformation behaviour of an idealised asphalt mixture", International Journal of Pavement Engineering, n. 5, pg. 1-7;
3. Cundall P.A. & Strack O.D.L. (1979), "A discrete numerical model for granular assemblies", Geotechnique,n. 29, pg. 47-65;
4. Cundall P.A., Ruest M.R., Guest A.R. & Chitombo G. (2003), "Evaluation of schemes to improve the efficiency of a complete model of blasting and rock fracture", Numerical Modelling in Micromechanics via Particle Methods, Konietzky H., A.A. Balkema, pg. 107-115;
5. Fwa T.F., Tan S.A. & Zhu L.Y. (2001), "Reexamining C-ϕ concept for asphalt paving mix design", Journal of Transportation Engineering, January-February, pg. 67-73.
6. Hainbüchner E., Potthoff S., Konietzky H. & Kamp L. (2003), "Particle based modelling of shear box tests and stability problems for shallow foundation in sand", Numerical Modelling in Micromechanics via Particle Methods, Konietzky H., A.A. Balkema, pg. 151-156;
7. Huebner K.H. (1995), "Finite element method for engineers", John Wiley and Sons;
8. Itasca (2002), "FLAC^{2D}: Fast Lagrangian Analysis of Continua", Version 4.0, Itasca Consulting Group;
9. Itasca (2002), "PFC^{2D}: Particle flow code in two dimensions", Version 3.0, Itasca Consulting Group;
10. Jing L. (2003), "A review of techniques, advances and outstanding issues in numerical modelling for rock mechanics and rock engineering", International Journal of Rock Mechanics & Mining Sciences, n. 40, pg. 283-353;
11. McDowell G.R. & Harireche O. (2002), "Discrete element modelling of yielding and normal compression of sand", Geotechnique, n. 4, pg. 299-304;
12. Zeghal M. (2004), "Discrete-Element Method Investigation of the Resilient Behaviour of Granular Materials", Journal of Transportation Engineering, July/August, pg. 503-509.